Clinical Neurophysiology Practice 9 (2024) 283–291

Contents lists available at ScienceDirect

Clinical Neurophysiology Practice

journal homepage: www.elsevier.com/locate/cnp

Research paper

Visualization of radial nerve activity at the upper arm using magnetoneurography

Takeyasu Toyama [a,*], Muneharu Ando [a], Masaaki Paku [a], Shinji Sato [b], Yusuke Yamamoto [b], Shinichirou Taniguchi [a], Nobuo Kohara [c], Takanori Saito [a]

[a] Department of Orthopedic Surgery, Kansai Medical University, 2-5-1 Shinmachi, Tokyo 101-0062, Japan
[b] RICOH Futures BU, RICOH Company, Ltd., 2-3-10 Kandasurugadai Chiyoda-ku, inamimachi, Chuo-ku, Kobe 650-0047, Japan
[c] Department of Neurology, Kobe City Medical Center General Hospital, 2-1-1 Minatojima M Hirakata, Osaka 573-1010, Japan

ARTICLE INFO

Keywords:
Evoked magnetic field
Magnetoneurography
Radial nerve

ABSTRACT

Objective: To evaluate the function of the radial nerve in the upper arm using Magnetoneurography (MNG).
Methods: Eight asymptomatic male volunteers (age 25–63 years) and one 67-year-old female patient with radial nerve palsy were included. The radial nerve was electrically stimulated in the right wrist, and the evoked magnetic field was recorded using a 132-channel bio-magnetometer system with a superconducting quantum interference device positioned below the upper arm. The measurements were divided into distal and proximal sessions because of the extensive range of the nerve.
Results: MNG recorded the radial nerve's evoked magnetic field in all cases, and the neural activity of the radial nerve at the upper arm was visualized using reconstructed currents. The mean conduction velocity calculated from the peak latency of the inward currents was 43.9 m/s for distal measurements and 57.9 m/s for proximal measurements. A 67-year-old female patient with radial nerve palsy had a disappearance of the reconstructed inward current and conduction disturbance of the axonal current, facilitating the identification of the lesion site.
Conclusions: MNG allowed visualization of the radial nerve activity in the upper arm and facilitated the identification of the lesion site in a patient with radial nerve palsy.
Significance: This method could be a useful diagnostic tool for patients with radial nerve palsy.

1. Introduction

Radial nerve palsy is frequently observed in daily orthopedic practice and can be caused by fractures of the humerus (Carroll et al., 2012) or compression near the spiral groove (Khedr et al., 2016). X-rays, MRI (Basta et al., 2014), and ultrasonography (Karabay et al., 2010) are used for morphological assessments, while electrophysiological examinations, such as nerve conduction studies (NCS) and electromyography, are used for functional nerve evaluation (Bumbasirevic et al., 2016). Motor or sensory conduction studies of the radial nerve involve placing recording electrodes on the extensor indicis proprius or the thumb and stimulating the radial nerve in the upper arm (Kimura, 2013). However, since the radial nerve runs deep around the humerus in a spiral pattern, it may be difficult to find a proper stimulation site (Jungho Yeo, 2017), making it more challenging to identify detailed lesion sites using the antidromic inching method compared to the carpal tunnel or cubital tunnel. Moreover, even with the orthodromic inching method, recording using surface electrodes at the upper arm level is impossible due to the deep pathway. Needle electromyography, which is useful for broadly identifying lesion sites, is invasive and has difficulty identifying detailed lesion sites. Therefore, a minimally invasive test that allows for a detailed neurofunctional evaluation of the lesion site is needed. Magnetoneurography (MNG) is a new functional imaging method for the nervous system that records magnetic fields generated according to Biot-Savart's law or Ampère's law after electrical nerve stimulation. Magnetoneurography (MNG) is a new functional imaging method for the nervous system that records magnetic fields generated according to Biot-Savart's law or Ampère's law after electrical nerve stimulation, enabling high-accuracy and high-resolution assessment of nerve function (Trahms et al., 2012). MNG can visualize nerve function by reconstructing the recorded magnetic field signals into current distributions. These features enable the assessment of the spinal cord and brachial plexus assessment, which are difficult to evaluate using traditional electrophysiological examinations. Previous reports have documented

* Corresponding author at: Department of Orthopedic Surgery, Kansai Medical University, 2-5-1 Shin-machi, Hirakata, Osaka 573-1010, Japan.
E-mail address: ttoyama1984@yahoo.co.jp (T. Toyama).

https://doi.org/10.1016/j.cnp.2024.11.001
Received 1 May 2024; Received in revised form 9 August 2024; Accepted 7 November 2024
Available online 15 November 2024

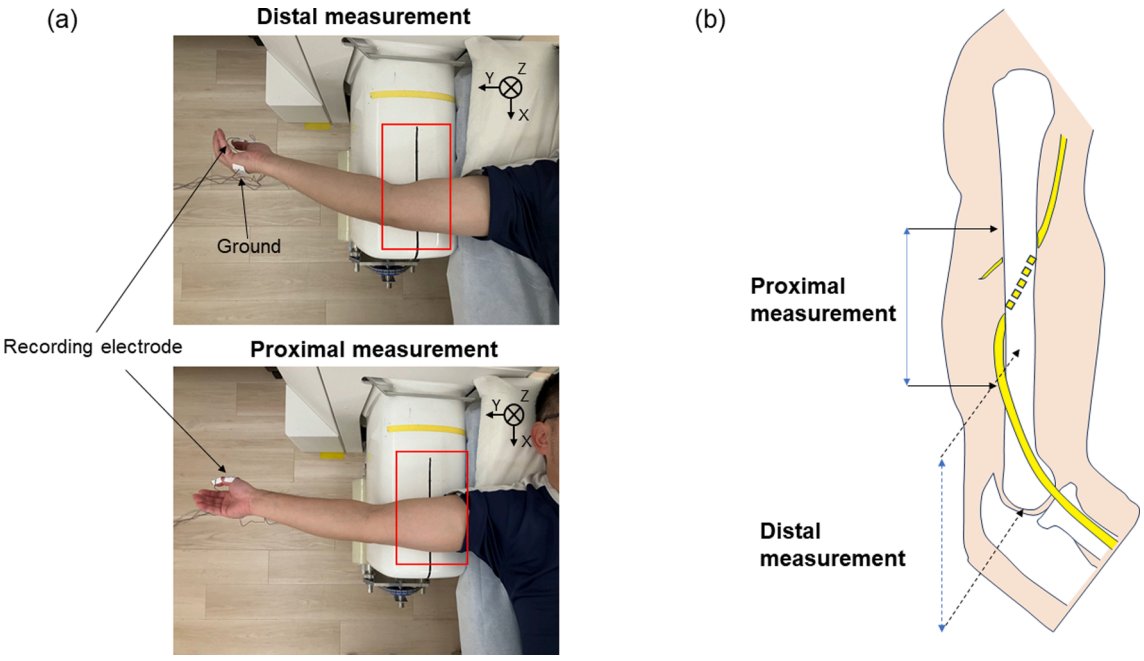

Fig. 1. Measurement methods and limb positioning. Participants placed their upper arms on the sensor. The squares indicate the measurement area. The magnetic field is measured by stimulating the radial nerve at the wrist. (a) Distal measurement: In the supine position, the shoulder was abducted to 90°, maximally externally rotated, and the elbow was extended. Proximal measurement: In the supine position, the shoulder was abducted to 90° with intermediate rotation, and the elbow was extended. (b) Illustration of the humerus and radial nerve with the measured area observed from the lateral side.

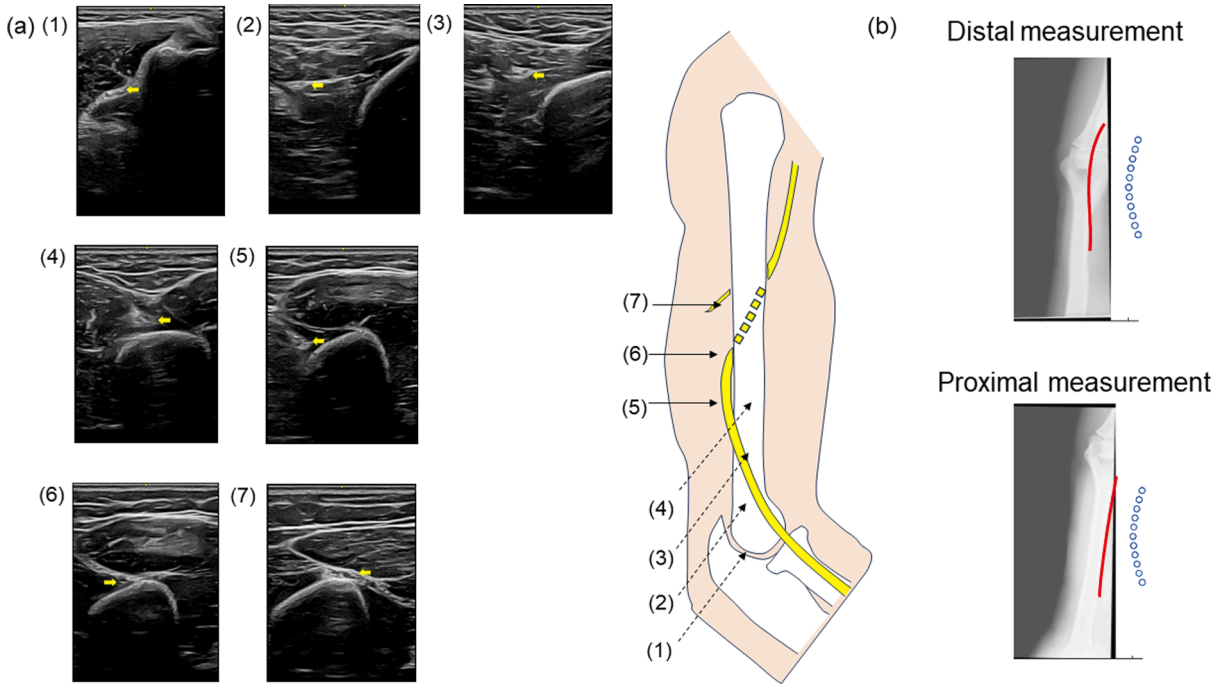

Fig. 2. Setting the Depth of the ROI.(a) Ultrasonography imaging within the measurement range. The yellow arrows indicate the cross-sections of the radial nerves. (1) shows an image at the elbow joint level in lateral view, and (2), (3), and (4) show images 3 cm, 6 cm, and 9 cm above the elbow joint, respectively. (5) is 9 cm above the elbow joint in the posterior view. (6) and (7) are located 12 and 15 cm above the elbow joint, respectively.(b) Lateral X-ray view in the distal measurement and the proximal one. The red line represents the depth of the region of interest (ROI). The blue circles indicate the positions of the sensors.

the visualization of neural activity in the spinal cord (Sumiya et al., 2017; Miyano et al., 2020), brachial plexus (Watanabe et al., 2019), and peripheral nerves in the carpal tunnel (Sasaki et al., 2022; Sato et al., 2023) and cubital tunnel (Hoshino et al., 2022). However, there have been no reports on the recording of the radial nerve activity using MNG, and the measurement method is not known. Visualization of radial nerve activity could potentially help identify detailed lesion sites in cases of radial nerve palsy, evaluate functional recovery, and aid in determining treatment strategies. This study aims to establish a measurement method for visualizing radial nerve activity using MNG. Additionally, we report on the use of MNG for a patient with radial nerve palsy.

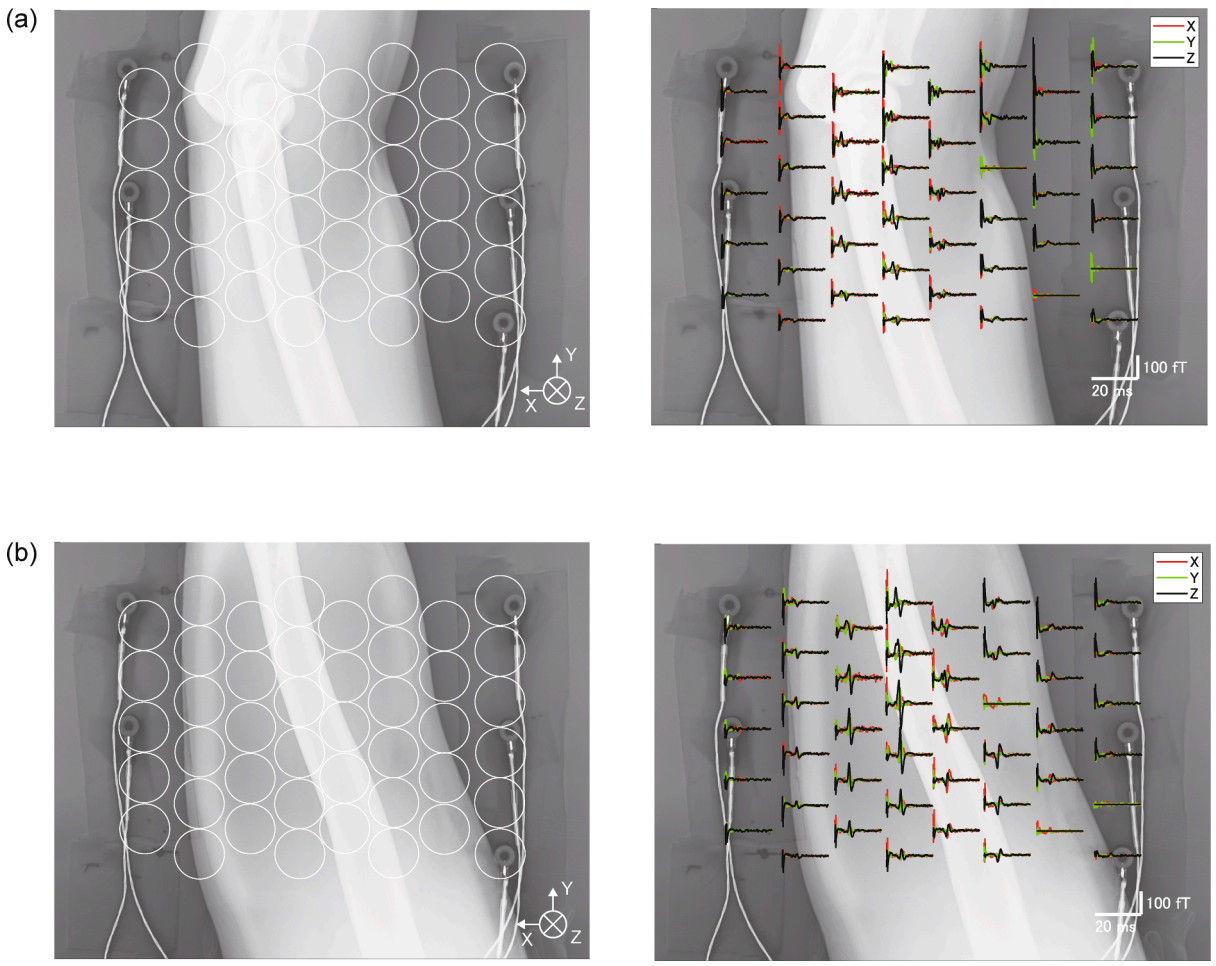

Fig. 3. Evoked magnetic field of the representative case. Evoked magnetic field was recorded from each sensor and the radiograph. The white circles represent the sensor positions. The red waveforms represent the magnetic field recorded from the X-directional coils, with the X-axis positively upward. The green waveforms represent the magnetic field recorded from the Y-directional coils, with the Y-axis positively upward. The black waveforms represent the magnetic field recorded from the Z-directional coils, with the direction towards the floor being positively upward. The polarity was reversed on both sides of the presumed radial nerve.

2. Methods

2.1. SQUID system

All the measurements were conducted in a magnetically shielded room. This room consists of multi-layer permalloy with high magnetic permeability, and its shielding factor is approximately 55 dB at 1 Hz in this measurement environment. Similar to that reported previously (Adachi et al., 2017), our MNG system consisted of a 132-channel (SQUID) biomagnetometer system developed by the Kanazawa Institute of Technology and Ricoh Company, Ltd. This system comprised an array of 44 SQUID sensors spaced 20–25 mm apart, covering an area of 180 mm × 130 mm. Each array was equipped with three orthogonal pickup coils that recorded the magnetic field in three orthogonal directions (X, Y, and Z). The typical noise level of the SQUID sensor was less than 4 $fT/Hz^{1/2}$ in the white region. The output of each SQUID sensor has a bandwidth above 5 kHz, and the output signal is filtered to 5 kHz.

2.2. Positional information

To obtain positional information between the magnetic sensors and the participants' bones, two-dimensional frontal and lateral X-ray images were taken. These radiographs were then superimposed on the sensor area. Additionally, two marker coils were placed under the participant's upper arm on the sensor. The position of these marker coils relative to the MNG sensors was determined from the generated magnetic fields. This approach allowed us to locate the participants in the recording area correctly.

2.3. Participants and recording of MNG

The study involved eight healthy male participants with no history of neurological disorders (mean age 35.8 years, range 25–63 years) and one 67-year-old female patient with radial nerve palsy. Recording electrodes were placed on the participants' thumbs, and electrical stimulation of the radial nerve at the wrist was performed to evoke maximal sensory nerve action potentials (SNAP) in the thumb (Fig. 1). The Neuropack X1 system (Nihon Kohden Inc., Tokyo, Japan) was used for electrical stimulation and recordings. The evoked magnetic fields were recorded using the MNG system with a 40 kHz sampling rate and a band-pass filter of 100–5000 Hz. The high-pass filter was set to 100 Hz to eliminate noise in the commercial power supply and system.

The measurements were divided into two sessions due to the extensive range of the nerve, covering the distal and proximal areas of the upper arm. The distal measurements included the elbow joint, whereas the proximal measurements covered up to 15 cm proximal to the elbow joint. For distal measurements, the arm was placed on the sensor in a supine position, with the shoulder abducted at 90° and maximally externally rotated, and the elbow extended (Fig. 1). For proximal measurements, the arm was placed on the sensor in a supine position, with the shoulder abducted at 90° and in intermediate rotation,

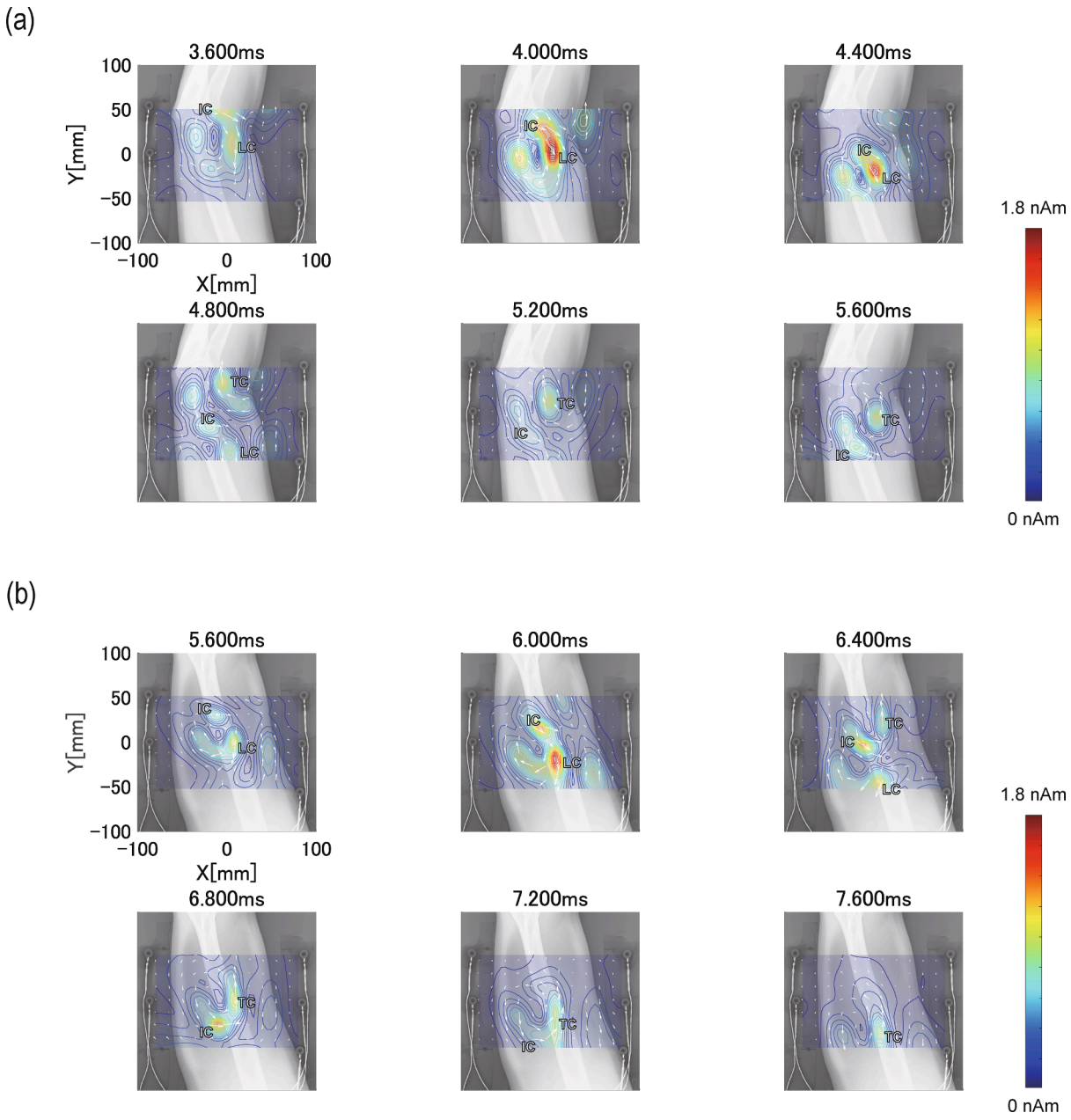

Fig. 4. Temporal and spatial changes in the equivalent current reconstructed by UGRENS in the representative case of a healthy participant.(a) Distal measurement: LC appeared at 3.6 ms and propagated proximally from 3.6 ms to 4.8 ms. IC appeared at 3.6 ms and also propagated proximally from 3.6 ms to 5.6 ms. TC appeared at 4.8 ms and propagated proximally from 4.8 ms to 5.6 ms. (b) Proximal measurement: LC appeared at 5.6 ms and propagated proximally from 5.6 ms to 6.4 ms. IC appeared at 5.6 ms and also propagated proximally from 5.6 ms to 7.2 ms. TC appeared at 6.0 ms and propagated proximally from 6.0 ms to 7.6 ms. The contour maps at 5.6 ms are shown for both distal and proximal measurements, but the current distributions appear different due to the different measurement positions of the limb.

and the elbow extended (Fig. 1). Each measurement yielded approximately 8,000 averages.

2.4. Signal Processing

The recorded magnetic fields were first processed using the dual-signal subspace projection (DSSP) algorithm to reduce artifacts (Sekihara et al., 2016; Sekihara and Nagarajan, 2017). Next, the data were processed using the unit gain constraint, recursively applied to null-steering spatial filtering (UGRENS) (Kumihashi and Sekihara, 2010; Sekihara and Nagarajan, 2015), which helped reconstruct the position and intensity of the currents. The evaluation of the reconstructed currents requires nerve depth information. Ultrasonography was used to measure the limb position before the examination, allowing us to determine the spatial relationship between the radial nerve and the humerus and the depth of the Region of Interest (ROI). Based on these findings, a nerve course related to the depth of the radial nerve was established on lateral radiographs taken before the examination. This process facilitated the accurate setting of the lateral nerve pathway on radiographs corresponding to the ROI (Fig. 2), enabling the reconstruction of the evoked currents on the plane of the ROI.

2.5. Ethics

All procedures in this study were approved by the Ethics Committee of our institute (approval no. 202048) and conducted in accordance with

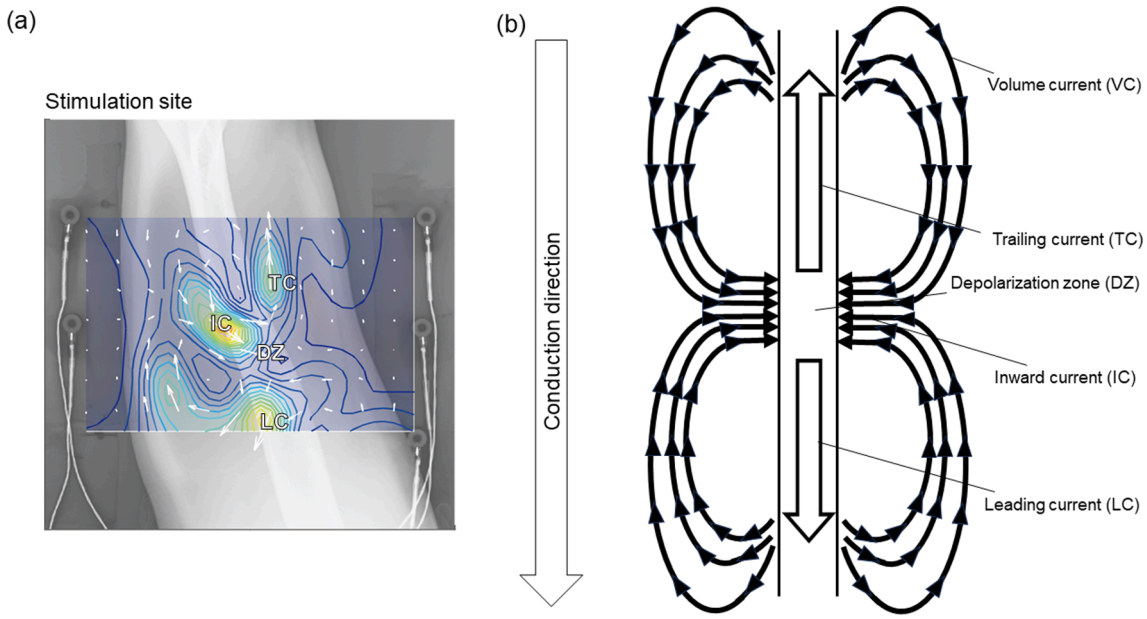

Fig. 5. Reconstructed current distribution and schematic diagram. (a) The contour map at 6.4 ms is shown in the same recording as in Fig. 4b. The top of the figure represents the stimulation side. Each white arrow in the current distribution indicates the direction of the current at that point. The color scale represents the current intensity (red indicating high intensity, blue indicating low intensity). (b) Current distribution schematic diagram: LC flows along the nerve axon in the direction of conduction, passes through the axon membrane from the front, veers away from the axon and then rotates around the subcutaneous volume conductor as VC before returning to DZ. Conversely, TC flows in the opposite direction to the direction of conduction within the nerve axon, crosses the membrane from the rear, moves within the subcutaneous volume conductor, and also returns to DZ. VC flowing into the DZ is referred to as IC.

the Declaration of Helsinki. Written informed consent and permission to publish images and photographs were obtained from all participants.

3. Results

3.1. Recording of evoked potentials and evoked magnetic fields

In all participants, evoked potentials following right radial nerve stimulation were recorded at the thumb, and the maximum intensity of stimulation was a mean of 7.1 mA (6–8) in healthy participants.

The evoked magnetic fields were recorded in response to the electrical stimulation in all cases. Fig. 3 shows the evoked magnetic fields in the X-, Y-, and Z-directions in a representative case. Magnetic fields in the Z-direction, generated by the intra-axonal current according to Ampere's law, reverse their polarity across the axon. In the magnetic field waveform of Fig. 3, the polarity is reversed in the Z-direction's magnetic field waveforms of the distal and proximal measurements, indicating that the radial nerve is present at that location. The maximum peak-to-peak magnetic field intensities recorded from each directional sensor for eight participants were as follows: for distal measurements, the mean values were 53.7 fT (range: 28.3–90.2) for the X-direction, 43.2 fT (range: 26.3–97.0) for the Y-direction, and 90.8 fT (range: 40.7–177.5) for the Z-direction. For proximal measurements, the mean values were 103.2 fT (range: 42.0–158.5) for the X-direction, 66.4 fT (range: 25.6–95.5) for the Y-direction, and 155.0 fT (range: 59.1–216.3) for the Z-direction.

3.2. Reconstructed current distribution in healthy participants

The reconstructed current distribution is shown as a color map superimposed on the radiograph of the humerus. In this study, a representative case of a healthy participants is presented (Fig. 4) Video 1.

Fig. 5a represents the current distribution at 6.4 ms in the recording shown in Fig. 4. The white arrows indicate the direction of the current at that point, and the color scale represents the intensity of the current (red indicates a high current, whereas blue indicates a low current). The current distribution of neural activity is shown in Fig. 5b. Current flows along the nerve axon from the depolarization zone (DZ) in both the anterior and posterior directions within the axon. The current flowing in the anterior direction was defined as the leading current (LC), and the current flowing in the posterior direction was defined as the trailing current (TC) (Nakayama et al., 2023). Volume currents flow outside the nerve axons towards the depolarization zone. The volume current flowing perpendicular to the depolarization zone is defined as the inward current (IC) (Fukuoka et al., 2002; Sasaki et al., 2020). Neural activity propagates from the stimulated site while maintaining this spatial relationship.

After stimulation of the radial nerve at the wrist, LC appeared at the elbow joint level at 3.6 ms (Fig. 4a), and the propagation of this current proximal along the course of the radial nerve was observed. At 4.8 ms, TC was also observed at the elbow joint (Fig. 4a), indicating the propagation of nerve activity. Additionally, the IC flowed perpendicularly between LC and TC on the dorsal side of the nerve. At 5.6 ms, the distal and proximal measurements, although measured at different limb positions, represented the current distribution of the same latency. Because the measurement limb positions were different, the reconstructed current distributions were different, even at the same latency. Propagation of neural activity was also observed in the proximal measurement of the upper arm (Fig. 4b).

3.3. Current waveforms calculated at virtual electrodes in healthy participants

Virtual electrodes were set along the radial nerve pathway, and the waveforms of currents parallel to the conduction path were calculated at intervals of 15 mm. Additionally, the waveforms of the IC were calculated at each virtual electrode set 20 mm dorsally from the conduction path.

In the representative measurements of healthy participants, propagation of the ICs was observed from the elbow joint to the proximal region. However, in distal measurements, the waveforms of electrodes 3

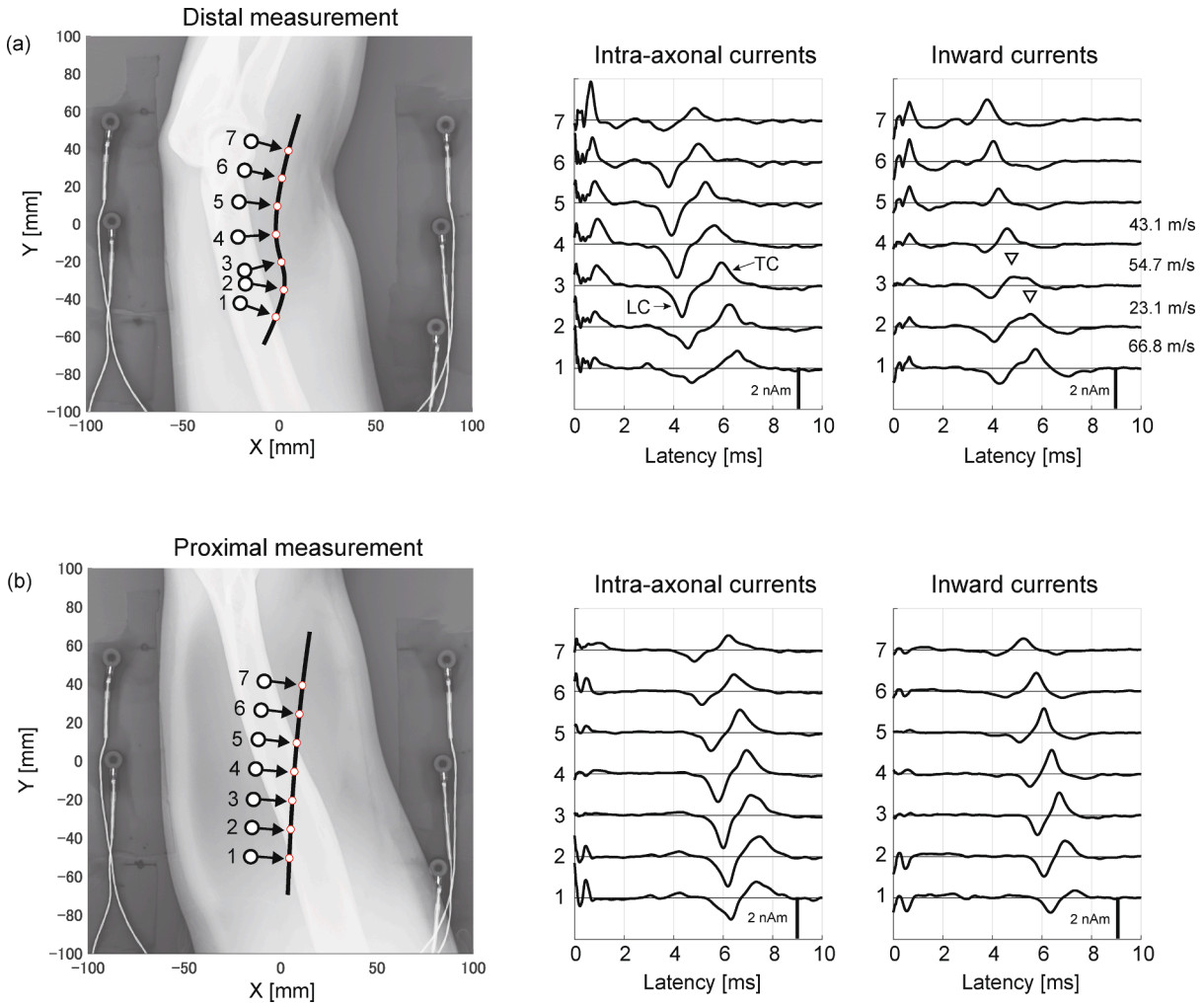

Fig. 6. Time course of reconstructed currents in a healthy participant. The reconstructed current was recorded using a virtual electrode from the same participant, as shown in Fig. 5. Intra-axonal currents and ICs propagate toward the proximal directions in both the distal (a) and proximal (b) measurements. Electrodes 1 in the distal measurement and 6 in the proximal measurement, respectively, exhibited the same IC latency peaks. In the distal measurement, the peaks of the IC waveforms of electrodes 3 and 2 (▽) were dull, and conduction velocities in this area decreased.

and 2 in the IC were slightly dull. Furthermore, the conduction velocity between virtual electrodes 3 and 2 was lower at 23.1 m/s compared to the other sections. Virtual electrodes 1 in the distal measurement and 6 in the proximal measurement had the same latency, and propagation of the ICs from distal to proximal was also observed in the proximal measurement (Fig. 6).

The mean conduction velocity of ICs in healthy participants was 43.9 m/s (39.3–47.2) in distal measurements and 57.9 m/s (46.1–71.7) in proximal measurements. The progression of the conduction velocity between each virtual electrode in all measurements of the healthy participants is presented in Fig. 7. Decreasing in conduction velocity was observed in the section from 4.5 cm to 7.5 cm above the elbow joint. The IC waveforms in those areas tended to become dull.

3.4. *Recording in a patient with radial nerve palsy*

The patient was a 67-year-old female. She experienced numbness from the right thumb to the middle finger and a wrist drop after waking up from a reclining chair. The symptoms did not improve, leading to consultation at our clinic two weeks after onset. Physical findings included numbness on the dorsal side of the right thumb to the middle finger and difficulty in active extension of the fingers and wrist. However, elbow extension was possible. Electrophysiological tests were performed for suspected radial nerve palsy. Needle electromyography showed active denervation in the extensor indicis proprius, extensor carpi radialis, and brachioradialis muscles, with reduced motor units and denervation potentials; however, no denervation potentials were observed in the triceps brachii and paraspinal muscles. The patient was diagnosed with radial nerve palsy based on the clinical symptoms and electromyographic findings. Four weeks after onset, the MNG of the radial nerve was measured.

Supramaximal stimulation of the radial nerve at the wrist was performed at 6.6 mA, and the evoked magnetic field was recorded. In the reconstructed current distribution, the LC appeared distally in the upper arm at 3.2 ms, and neural activity propagated proximally. However, at 3.6 ms, LC spread widely in the conduction direction, and after that, the signal intensity weakened at 4.0 ms and disappeared at 4.4 ms. IC was also observed in the distal upper arm at 3.2 ms and propagated proximally. However, the signal weakened at 4.4 ms and subsequently disappeared (Fig. 8). In current waveforms calculated at virtual electrodes (Fig. 9), the IC was attenuated at virtual electrode 3 and became extremely small at electrode 2. The latency of LC and IC peaks for virtual electrodes 2 and 1 were almost the same as those for virtual electrodes 3. In other words, the propagation of neural activity appeared to stop near the virtual electrode 3. These results suggested lesion sites between virtual electrodes 3 and 1.

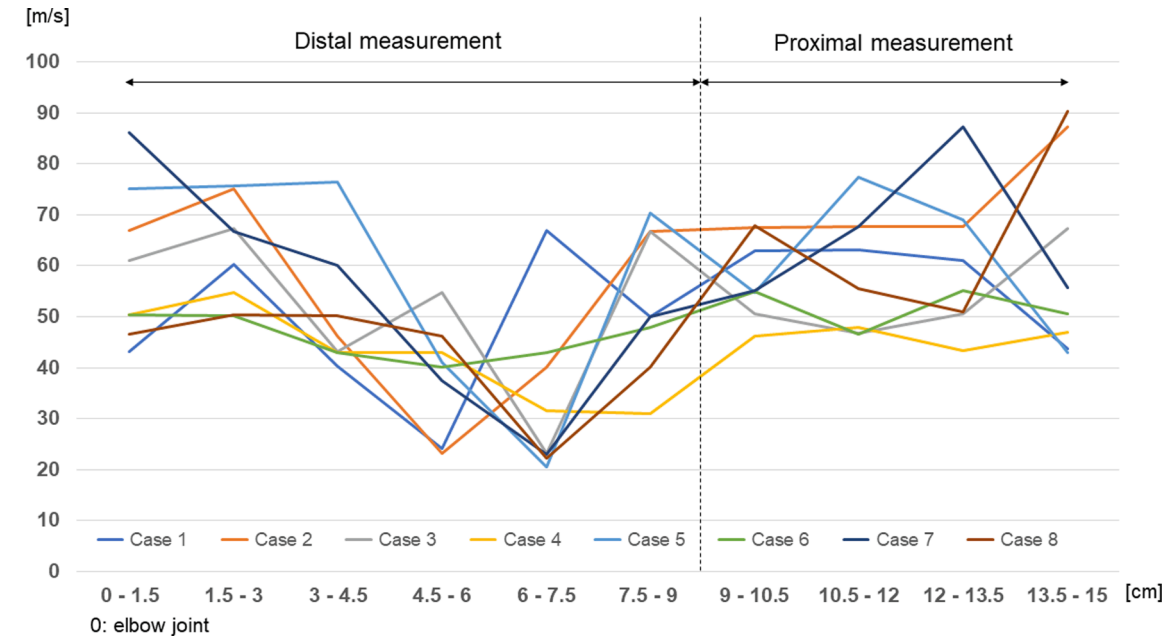

Fig. 7. Consecutive change in conduction velocity between each electrode in all healthy participants. The horizontal axis indicates the consecutive sections from the elbow joint (0 cm): the data of 0–9 cm was taken from the distal measurement and those 9–15 cm from the proximal measurement. The vertical axis represents the conduction velocity in each section. A tendency for conduction delay was observed from 4.5 cm to 7.5 cm above the elbow joint.

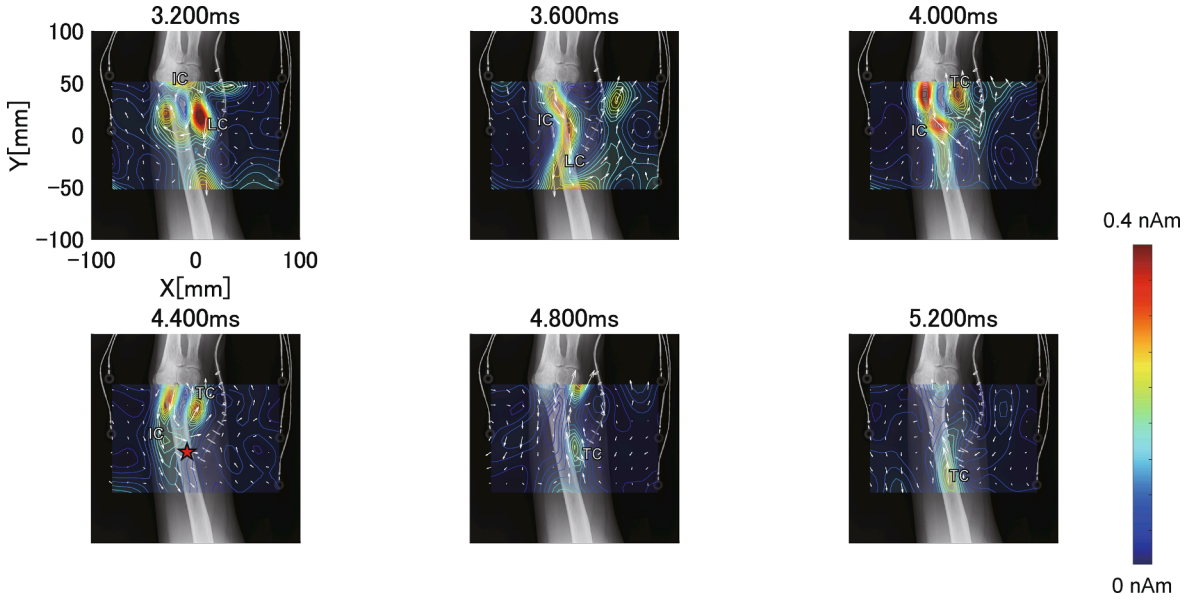

Fig. 8. Temporal and spatial changes in the equivalent current reconstructed by UGRENS in a patient with radial nerve palsy. LC appeared at 3.2 ms, and the neural activity propagated proximally. However, at 3.6 ms, LC was observed to spread widely in the conduction direction, and then signal intensity weakened at 4.0 ms and disappeared at 4.4 ms. IC was also observed in the distal upper arm at 3.2 ms and propagated proximally, but the signal intensity of IC weakened at 4.4 ms and subsequently disappeared. The red star indicates the lesion site.

4. Discussion

In this study, we successfully visualized the radial nerve activity using MNG. The radial nerve runs deep around the humerus in a spiral, making the detailed evaluation of lesion sites more challenging compared to inching methods used for the carpal tunnel and cubital tunnel regions. However, using MNG allows for easy and detailed neurofunctional evaluations, and in cases of radial nerve palsy, it enables the identification of lesion sites. This study is the first report to evaluate the function of the radial nerve using MNG.

The magnetic field signal obtained during distal measurements was small because the distance from the sensor to the nerve was greater, averaging 53.7 fT on the X directional sensor, 43.2 fT on the Y directional sensor, and 90.8 fT on the Z directional sensor, necessitating 8000 stimulations. The magnetic field signal obtained during proximal measurements was relatively larger, averaging 103.2 fT on the X directional sensor, 66.4 fT on the Y directional sensor, and 155.0 fT on the Z directional sensor, so 4000 stimulations might have been sufficient. However, due to the participants' larger upper arm circumference, which increased the distance between the sensor and the nerve, there were cases where the magnetic field signal was small, even in proximal measurements. Additionally, in actual patient measurements, the

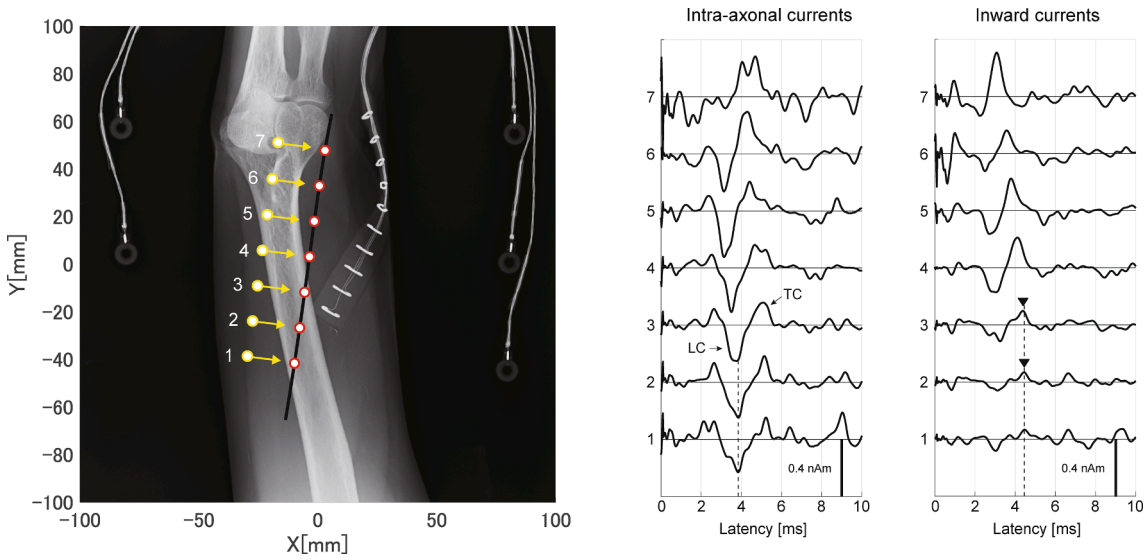

Fig. 9. Time course of reconstructed currents in a patient with radial nerve palsy. IC was attenuated at virtual electrode 3 and became extremely small at electrode 2 (▼). The latency of LC and IC peaks for virtual electrodes 2 and 1 (dotted line) were almost the same as those for virtual electrode 3. In other words, the propagation of the neural activity appeared to stop near the virtual electrode 3.

magnetic field signal obtained may be smaller than that of healthy participants, so 8000 stimulations were used.

According to previous reports, the IC is thought to represent volume currents following the DZ (Fukuoka et al., 2002; Sasaki et al., 2020; Nakayama et al., 2023). In this study's measurements of healthy participants, propagation of the ICs from distal to proximal was observed in all cases. The mean conduction velocity of ICs was 43.9 m/s for distal measurement and 57.9 m/s for proximal measurement.

A tendency for a conduction delay was observed in the section from 4.5 cm to 7.5 cm above the elbow joint when measuring the conduction velocity progression between each virtual electrode in healthy participants. This conduction delay may be because the radial nerve pathway in this area undergoes rapid three-dimensional changes before entering the spiral groove. Indeed, in the reconstructed current distribution, the conduction path of the axonal current exhibited rapid changes within this section (Fig. 6a) Video 1. These rapid changes might be attributed to the challenge of accurately establishing the nerve pathway in this area, making it difficult to measure the distance between the electrodes. Another reason is that the MNG calculates evoked currents from magnetic signals rather than from actual currents. Magnetic signals with opposite vectors can cancel each other out, creating an absence of current (Hashimoto et al., 2022). This phenomenon may occur in areas where the nerves run in a deep direction. In fact, electrodes 3 and 2 of the IC show a dull waveform in this area, as shown in Fig. 6a. It may be difficult to obtain the magnetic field signal accurately in this area. Although the exact cause is unclear, understanding the apparent conduction delay in this area is crucial. Therefore, evaluating both the current distribution and waveforms with this understanding is necessary.

In the measurements of patients with radial nerve palsy, it was possible to identify detailed lesion sites due to the disappearance of the IC or disturbances in the LC. This method may prove useful in identifying detailed lesion sites in patients with radial nerve palsy in the future.

This study had several limitations. First, this method may not be useful in severe cases of axonal degeneration. It is necessary to verify methods for measuring magnetic fields using stimulation proximal to the measurement site, such as the measurement of the carpal tunnel region using elbow stimulation (Sato et al., 2023).

Second, the radial nerve runs deep in a spiral pattern around the humerus, making it difficult to set the depth of the Region of Interest (ROI). In this study, due to the change in radial nerve depth depending on the position of the upper limb and the ease of measuring nerve depth, ultrasonography was used to confirm the course of the radial nerve at the measurement position and set the depth of the ROI. However, in previous reports on MNG (Sasaki et al., 2020), MRI has been used to set the depth of the ROI. It may be necessary to verify which method can set the depth more accurately and is more useful.

Third, this method involves stimulation of the sensory branch of the radial nerve at the wrist. Hence, it is possible to use it to evaluate the nerve function of the radial nerve in the upper arm. However, the posterior interosseous nerve has not been evaluated. It is necessary to continue exploring methods to evaluate the function of the posterior interosseous nerve. Consequently, the development of a method to evaluate the function of the posterior interosseous nerve presents a significant challenge for future studies.

5. Conclusion

The radial nerve activity of the upper arm can be visualized using an MNG. Additionally, MNG allows the identification of detailed lesion sites in patients with radial nerve palsy. MNG enables the evaluation of the radial nerve function and may be used for the detailed diagnosis of lesion sites in patients with radial nerve palsy.

Author contributions

T.T., M.A., M.P., S.S., and Y.Y contributed to the project's initial concept and design. T.T., M.A., M.P., S.S., and Y.Y carried out the practical implementation and operational tasks. The data analysis and its interpretation were conducted by T.T., M.A., M.P., S.S., Y.Y., N.K., S. T., and T.S. This manuscript has received endorsement for submission from all participating authors.

Funding

RICOH Company, Ltd supported this work. The funding source had no role in study design, data collection and analysis, preparation of the manuscript, or the decision to publish.

Declaration of competing interest

The authors declare that they have no known competing financial interests or personal relationships that could have appeared to influence the work reported in this paper.

Appendix A. Supplementary data

Supplementary data to this article can be found online at https://doi.org/10.1016/j.cnp.2024.11.001.

References

Adachi, Y., Kawai, J., Haruta, Y., Miyamoto, M., Kawabata, S., Sekihara, K., Uehara, G., 2017. Recent advancements in the SQUID magnetospinogram system. Supercond. Sci. Technol. 30, 6. https://doi.org/10.1088/1361-6668/aa66b3.

Basta, I., Nikolić, A., Apostolski, S., Lavrnić, S., Stosić-Opinćal, T., Banjalić, S., Knezević-Apostolski, S., Ilić, T.V., Marjanović, I., Milićev, M., Lavrnić, D., 2014. Diagnostic value of combined magnetic resonance imaging examination of brachial plexus and electrophysiological studies in multifocal motor neuropathy. Vojnosanit. Pregl. 71, 723–729. https://doi.org/10.2298/vsp1408723b.

Bumbasirevic, M., Palibrk, T., Lesic, A., Atkinson, H.D.E., 2016. Radial Nerve Palsy. EFORT Open Rev. 1, 286–294. https://doi.org/10.1302/2058-5241.1.000028.

Carroll, E.A., Schweppe, M., Langfitt, M., Miller, A.N., Halvorson, J.J., 2012. Management of humeral shaft fractures. J. Am. Acad. Orthop. Surg. 20, 423–433. https://doi.org/10.5435/JAAOS-20-07-423.

Fukuoka, Y., Komori, H., Kawabata, S., Ohkubo, H., Shinomiya, K., Terasaki, O., 2002. Imaging of neural conduction block by neuromagnetic recording. Clin. Neurophysiol. 113, 1985–1992. https://doi.org/10.1016/s1388-2457(02)00345-0.

Hashimoto, J., Kawabata, S., Sasaki, T., Hoshino, Y., Sekihara, K., Adachi, Y., Watanabe, T., Miyano, Y., Mitani, Y., Sato, S., Kim, S., Yoshii, T., Okawa, A., 2022. Assessment of thoracic spinal cord electrophysiological activity through magnetoneurography. Clin. Neurophysiol. 133, 39–47. https://doi.org/10.1016/j.clinph.2021.09.023.

Hoshino, Y., Kawabata, S., Adachi, Y., Watanabe, T., Sekihara, K., Sasaki, T., Hashimoto, J., Fujita, K., Nimura, A., Okawa, A., 2022. Magnetoneurography as a novel functional imaging technique for the ulnar nerve at the elbow. Clin. Neurophysiol. 138, 153–162. https://doi.org/10.1016/j.clinph.2022.03.017.

Jungho, Y., Yuntae, K., Sooa, K., Kiyoung, O., Hyungdong, K., 2017. Optimal radial motor nerve conduction study using ultrasound in healthy adults. Ann. Rehabil. Med. 41, 290–298. https://doi.org/10.5535/arm.2017.41.2.290.

Karabay, N., Toros, T., Ademoğlu, Y., Ada, S., 2010. Ultrasonographic evaluation of the iatrogenic peripheral nerve injuries in upper extremity. Eur. J. Radiol. 73, 234–240. https://doi.org/10.1016/j.ejrad.2008.10.038.

Khedr, E.M., Fawi, G., Abbas, M.A., Abo El-Fetoh, N., Zaki, A.F., Gamea, A., Al Attar, G., 2016. Prevalence of neuromuscular disorders in Qena Governorate/Egypt: population-based survey. Neurol. Res. 38, 1056–1063. https://doi.org/10.1080/01616412.2016.1243640.

Kimura, J., 2013. Electrodiagnosis in diseases of nerve and muscle: principles and practice. Oxford University Press, New York. https://doi.org/10.1093/med/9780199738687.001.0001.

Kumihashi, I., Sekihara, K., 2010. Array-gain constraint minimum-norm spatial filter with recursively updated gram matrix for biomagnetic source imaging. IEEE Trans. Biomed. Eng. 57, 1358–1365. https://doi.org/10.1109/TBME.2010.2040735.

Miyano, Y., Kawabata, S., Akaza, M., Sekihara, K., Hoshino, Y., Sasaki, T., Watanabe, T., Kim, S., Sato, S., Mitani, Y., Adachi, Y., Okawa, A., 2020. Visualization of electrical activity in the cervical spinal cord and nerve roots after ulnar nerve stimulation using magnetospinography. Clin. Neurophysiol. 131, 2460–2468. https://doi.org/10.1016/j.clinph.2020.07.009.

Nakayama, K., Kohara, N., Paku, M., Sato, S., Nakamura, M., Ando, M., Taniguchi, S., Ishihara, M., Tani, Y., Itakura, T., Saito, T., Yakushiji, Y., 2023. Visualization of axonal and volume currents in median nerve compound action potential using magnetoneurography. Clin. Neurophysiol. 152, 57–67. https://doi.org/10.1016/j.clinph.2023.05.006.

Sasaki, T., Kawabata, S., Hoshino, Y., Sekihara, K., Adachi, Y., Akaza, M., Ozaki, I., Fujita, K., Nimura, A., Yoshii, T., Miyano, Y., Mitani, Y., Watanabe, T., Sato, S., Kim, S., Okawa, A., 2020. Visualization of electrophysiological activity at the carpal tunnel area using magnetoneurography. Clin. Neurophysiol. 131, 951–957. https://doi.org/10.1016/j.clinph.2019.11.030.

Sasaki, T., Kawabata, S., Hashimoto, J., Hoshino, Y., Sekihara, K., Adachi, Y., Akaza, M., Fujita, K., Nimura, A., Yoshii, T., Miyano, Y., Mitani, Y., Watanabe, T., Sato, S., Kim, S., Okawa, A., 2022. Assessing carpal tunnel syndrome with magnetoneurography. Clin. Neurophysiol. 139, 1–8. https://doi.org/10.1016/j.clinph.2022.03.021.

Sato, S., Akaza, M., Sasaki, T., Tanaka, Y., Hashimoto, J., Watanabe, T., Miyano, Y., Kim, S., Kaminaka, S., Sumi, Y., Sekihara, K., Adachi, Y., Kawabata, S., 2023. Evaluation of electrical activity at the carpal tunnel area in response to median nerve elbow stimulation using magnetoneurography. Clin. Neurophysiol. 156, 89–97. https://doi.org/10.1016/j.clinph.2023.09.016.

Sekihara, K., Kawabata, Y., Ushio, S., Sumiya, S., Kawabata, S., Adachi, Y., Nagarajan, S. S., 2016. Dual signal subspace projection (DSSP): a novel algorithm for removing large interference in biomagnetic measurements. J. Neural Eng. 13, 036007. https://doi.org/10.1088/1741-2560/13/3/036007.

Sekihara, K., Nagarajan, S.S., 2015. Electromagnetic brain imaging, a Bayesian perspective. Springer International Publishing, Cham, Switzerland. https://doi.org/10.1007/978-3-319-14947-9.

Sekihara, K., Nagarajan, S.S., 2017. Subspace-based interference removal methods for a multichannel biomagnetic sensor array. J. Neural Eng. 14, 051001. https://doi.org/10.1088/1741-2552/aa7693.

Sumiya, S., Kawabata, S., Hoshino, Y., Adachi, Y., Sekihara, K., Tomizawa, S., Tomori, M., Ishii, S., Sakaki, K., Ukegawa, D., Ushio, S., Watanabe, T., Okawa, A., 2017. Magnetospinography visualizes electrophysiological activity in the cervical spinal cord. Sci. Rep. 7, 2192. https://doi.org/10.1038/s41598-017-02406-8.

Trahms, L., Erné, S.N., Trontelj, Z., Curio, G., Aust, P., 1989. Biomagnetic functional localization of a peripheral nerve in man. Biophys. J. 55, 1145–1153. https://doi.org/10.1016/S0006-3495(89)82911-X.

Watanabe, T., Kawabata, S., Hoshino, Y., Ushio, S., Sasaki, T., Miyano, Y., Ozaki, I., Adachi, Y., Sekihara, K., Okawa, A., 2019. Novel functional imaging technique for the brachial plexus based on magnetoneurography. Clin. Neurophysiol. 130, 2114–2123. https://doi.org/10.1016/j.clinph.2019.08.006.